

Representation Abstractions as Incentives for Reinforcement Learning Agents: A Robotic Grasping Case Study

Panagiotis Petropoulakis^{1*}, Ludwig Gräf^{1*}, Josip Josifovski^{1†}, Mohammadhossein Malmir^{1†}, and Alois Knoll¹

Abstract—Choosing an appropriate representation of the environment for the underlying decision-making process of the reinforcement learning (RL) agent is not always straightforward. The state representation should be inclusive enough to allow the agent to informatively decide on its actions and compact enough to increase sample efficiency for policy training. Given this outlook, this work examines the effect of various state representations in incentivizing the agent to solve a specific robotic task: antipodal and planar object grasping. A continuum of state representation abstractions is defined, starting from a model-based approach with complete system knowledge, through hand-crafted numerical, to image-based representations with decreasing level of induced task-specific knowledge. We examine the effects of each representation in the ability of the agent to solve the task in simulation and the transferability of the learned policy to the real robot. The results show that RL agents using numerical states can perform on par with non-learning baselines. Furthermore, we find that agents using image-based representations from pre-trained environment embedding vectors perform better than end-to-end trained agents, and hypothesize that task-specific knowledge is necessary for achieving convergence and high success rates in robot control. Supplementary material can be found at the project webpage².

I. INTRODUCTION

If we consider state representations in reinforcement learning for robot control, the representation space \mathcal{F} can be partitioned into two sub-spaces: the Vision State Space \mathcal{V} where the agent receives raw image data, and the Numerical State Space \mathcal{N} where the agent relies on hand-crafted states (e.g., derived from the robot encoders or pre-processed raw sensor data) suitable for the task. While the raw image data is more general representation, it is often not directly useful as-is, since it contains unprocessed and dense information that could hinder the learning process. For example, a significant gap in performance was evident in the DeepMind Control Suite [1] between numerical and vision-based states, where agents trained directly on images required, on average, more than 60 million steps to reach convergence, while harder tasks could not be solved at the same level compared to agents that rely on hand-crafted numerical states.

¹ The authors are with the Department of Computer Engineering, School of Computation, Information and Technology, Technical University of Munich, Germany.

* Panagiotis Petropoulakis and Ludwig Gräf are co-first authors.

† Josip Josifovski and Mohammadhossein Malmir are co-second authors.

This work has been financially supported by A-IQ READY project, which has received funding within the Key Digital Technologies Joint Undertaking (KDT JU) - the Public-Private Partnership for research, development and innovation under Horizon Europe – and National Authorities under grant agreement No. 101096658.

²<https://github.com/PetropoulakisPanagiotis/igae>

Consequently, the creation of concise representations, often called observation incentives [2], necessitates the identification and selection of the most essential and informative elements available from the environment. To do this, intervention incentives are used to influence observation incentives by changing the conditional probability distribution of the node [3], and hopefully, enriching the representation and accelerate exploration [4]. Intervention incentives can be, for example, additional objectives for the task, designing of specific neural network architectures, or added randomization noise to the observations.

Plenty of works in reinforcement learning for robotics use such incentives to shape the state representation for the RL agent. However, there is rarely a comparison of how different state representations would influence the performance of the agent, or even more importantly in the context of simulation-based robot learning, how the representation influences the transferability of the model to the real system. To provide some insight into these questions, in this work we consider a continuum of state representations for a robotic grasping task, ranging from a hand-crafted numerical state to an abstract representation that should be learned from raw image data. An objective comparison has been made to assess which of the approaches are more suitable based on the specific requirements of the task, available system and environment information, and the level of robust transferability required for real-world applications. Our analysis shows that when high performance and smooth sim-to-real transfer is necessary, general representations that do not include domain knowledge are under-performing. To address this problem, we propose the Incentivized Grasping AutoEncoder (IGAE) architecture, an image-based approach that introduces domain-specific knowledge and enhances the agent’s performance while maintaining a general representation.

II. BACKGROUND AND RELATED WORK

When one defines the state for the RL agent, this definition might be more tailored to the specific task and reward-driven [5], or it can be reward-free and involve unsupervised, self-supervised, or pre-trained models to create more generic features. For reward-free methods, there are numerous paradigms for extracting meaningful representations. In [6], the authors examined how Maximum Likelihood Estimation (MLE) can approximate the dynamics of data distributions that originate from exploratory policies, ultimately leading to the learning of a low-dimensional feature representation. Other approaches [7], [8] involve the utilization of adversarial losses, where a minimax objective is formulated, after which

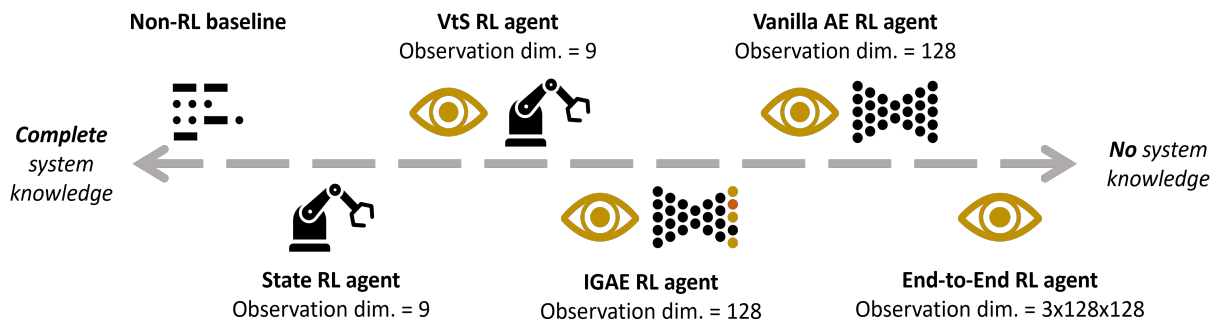


Fig. 1: A model-based baseline with full system knowledge and multiple reinforcement learning approaches based on different state representation spaces with decreasing level of system knowledge (increasing abstraction) are examined in this analysis. Models on the left have the state information explicitly available in the form of numerical values for the robot joints or the object, whereas on the right, vision-centric techniques generate implicit latent representation to guide the RL policy.

standard gradient-based methods are employed to optimize the discriminators’ functions responsible for generating the state abstractions.

To address the challenge of data efficiency and generalization to new environments in both vision-based and hand-crafted numerical representations, recent efforts have introduced data augmentation techniques borrowed from the computer vision domain [1]. The Reinforcement Learning with Augmented Data (RAD) module [9] showed that even basic randomization added to state abstractions alone outperforms more complex methods, such as pixel SAC [10].

While randomization can improve the performance, in some cases it can also increase the complexity of the task and hinder the optimization process. In [11], the effects of randomization in numerical-based agents for sim-to-real transfer of a robotic reaching task were analysed. The results showed that the randomization helps in sim-to-real transfer, but inappropriate randomization ranges can prevented the agent from finding a good policy.

Recently, several works have focused on decoupling the perception module from the policy and reducing the computational overhead of RL training, with the aim of addressing more complex tasks. Parisi et al. [12] demonstrated the effectiveness of general pre-trained feature embeddings from ImageNet [13] used to train a shallow Multi-Layer Perceptron (MLP) policy. This approach successfully solved several tasks, where an end-to-end visuo-motor policy failed. In [14], the authors combined multi-view image observations and visio-motor feedback through a Grasp Q-Network. The state abstraction of the RL agent involved a latent feature vector derived from convolutional and fully-connected layers. This representation enabled a 7-DOF Baxter robot to achieve a grasping accuracy of over 90% for specific object categories.

Due to their unsupervised nature, autoencoders have also emerged as a key architecture for implementing the perception module in reinforcement learning for robotic tasks. Breyer et al. [15] presented an autoencoder-based approach to map a masked input image of an object of interest to a low-dimensional vector, and defined an efficient and dense reward function with a prioritized RL sampling scheme to curate

difficult cases during training. This approach achieved high success rates in tasks involving picking and lifting objects. In the work by Nair et al. [16], a Context-Conditional Variational Autoencoder (CC-VAE) network was trained while taking both an input condition, the goal image observation, and the image of the current state observation into account. The reward signal for the RL agent was then directly defined within this latent space. This formulation allowed users to specify the goal condition (image) during testing, enabling the robotic system to push an object to the desired position. Similarly, Zhan et al. [17] utilized learned latent vectors extracted from an autoencoder trained in a contrastive manner. They combined several data augmentation techniques and demonstration paradigms and then optimized a policy in just 30 minutes to control a manipulator capable of performing diverse tasks, including pulling large objects, and opening drawers.

III. METHODOLOGY

In this section, we start by formally defining a task suitable for comparing different state representations. We then explain in detail the image processing architecture for the vision-based representations, the randomization observation incentives for sim-to-real transfer, and finally, the evaluation process.

A. Task Formulation

The task is to learn a control policy for a robotic manipulator to perform an antipodal grasp of an object placed at a random position in its workspace. The manipulator with seven DoF is controlled in task space.

More formally, the RL agent learns to command the actions as specified by:

$$a_t = [v_{x_t}, v_{y_t}] \in \mathbb{R}^2 \quad (1)$$

After the agent completes the RL episode, predefined actions are applied to attempt grasping. Namely, if there are no collisions at the conclusion of the episode, the following manual actions are initiated: 1) move down to a predetermined height, 2) close the gripper, and 3) move up to a predetermined height. Therefore, a successful grasping can only occur if the

end effector is in the ideal position before the start of the manual actions. If a collision occurs at any point, a penalty is added once in the total return, and the episode is considered unsuccessful. This penalty is applied only when: 1) there is a collision of the fingers with the object, 2) there is a collision of the robot with itself, or 3) the safety limit of the joints is violated. For the remaining steps of the episode, the RL agent receives zero reward, with zero velocities commanded to the manipulator.

More formally, the reward function that guides the agent in learning the task is structured as follows:

$$r_t = \begin{cases} w_x * \Delta d_{x_t} + w_y * \Delta d_{y_t}, & \text{no collision} \\ r_c, & \text{collision} \end{cases} \quad (2)$$

where we have t ranging from 0 to N , representing the episode time step, with N denoting the episode duration. Δd_{x_t} and Δd_{y_t} are the normalized differences in errors between the distance from the end effector to the object in the x and y -axes at the current time step compared to the previous one. In particular, Δd_{x_t} is equivalent to $(\delta_{x_{t-1}} - \delta_{x_t})$. Here, δ_{x_t} is the distance of the end effector to the object at time step t and $\delta_{x_{t-1}}$ is the distance at $t - 1$, the previous time step³.

B. Image Processing Backbone

To examine vision-based approaches and mitigate the high training time disparities compared to the numerical agents, while also ensuring fair comparisons across methods, image observations are pre-processed by the same encoder, as depicted in Figure 2. The output then represents the input state for the RL agent. Nevertheless, to create distinct representation abstractions, we introduce variations in the training objectives. This approach allows us to gain deeper insights into how intervention observation incentives can transform the original space into a more meaningful and sample-efficient space for the policy to learn the task.

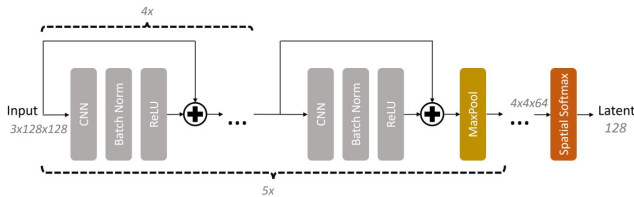


Fig. 2: The same backbone architecture was consistently used in all of the vision-based RL agents. This decision was made to assess the impact of various training objectives in shaping the original image space \mathcal{V} into meaningful representation abstractions of the environment. The architecture itself is an adaption of the ResNet Autoencoder (AE) [18] with a spatial softmax output layer [19], [20].

³In the analysis, we found that the best performance was achieved by separating the errors of the two axes into distinct terms. The conventional practice of using the negative Euclidean distance from the end effector to the object as a reward for grasping led to significantly slower convergence compared to our modification.

C. State Representation Abstractions

Six representation abstraction spaces are formulated in this and the next section to train RL agents through the reward function and compared with a non-RL baseline. The methods vary from predefined hard-coded spaces to a more general end-to-end paradigm, as shown in Figure 1.

Non-RL Baseline: The baseline method employed is Ruckig, a real-time, open-source, and time-optimal trajectory generation algorithm described in [21]. The baseline has full system knowledge, and therefore, it serves as an upper bound for the performance of the RL agents.

State RL Agent: The first learning agent and the simplest state representation abstraction is implemented through a hard-coded numerical approach. This particular agent, denoted as the State RL agent, relies on the manipulator’s encoder measurements, and its state space is defined as follows:

$$s_t = [\Delta x_t, \Delta y_t, q_{1_t}, \dots, q_{7_t}] \in \mathbb{R}^9, \quad (3)$$

In this context, Δx_t and Δy_t are the positional errors between the end effector and the target position of the box in x and y -axes, while q_{i_t} is the i -th joint position of the manipulator.

Vision-to-State RL Agent: The Vision-to-State (VtS) RL agent represents the transition between numerical and image-based representations. Rather than relying on the manipulator’s encoders, the joint angles and the positional errors, as described above, are predicted here from image observations. The convolutional backbone (see section III-B), processes RGB images and a shallow MLP consisting of 4 layers is pre-trained to predict the numerical state of the agent.

Incentivized Grasping AutoEncoder RL Agent: The next level of state abstraction is an autoencoder-based latent representation derived from image observations. To achieve a balanced blend of general representation and task-specific precision, we introduce the Incentivized Grasping AutoEncoder (IGAE) architecture (see Figure 3.). The IGAE is a segmentation-inspired RL agent tailored for the grasping task by introducing additional objectives, i.e. intervention observation incentives. These incentives are designed with the intention of isolating and shaping specific regions of the vision space \mathcal{V} , guiding the RL agent to learn the task in a more sample-efficient manner.

Vanilla AutoEncoder RL Agent: In this level of abstraction, we are now progressively eliminating human-injected knowledge, and shifting to a more abstract and generic representation. For the vanilla AE agent, we discard the extra objectives introduced in the IGAE agent, and retain only the RGB reconstruction head to project the vision space into a more generic latent feature representation.

End-to-End RL Agent: In the most extreme case of defining a representation space, we grant complete freedom to the RL policy. We couple representation learning with the policy learning step and update the vision module’s weights as the agent learns the grasping task. The primary goal of the end-to-end RL agent is to learn the task relying

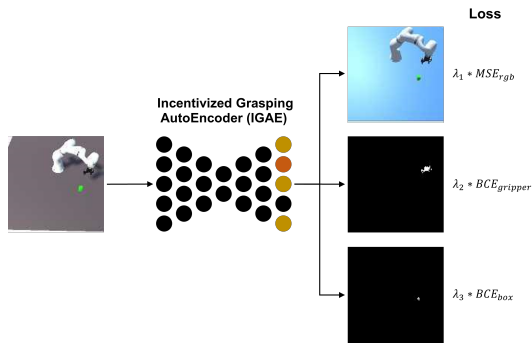


Fig. 3: The Incentivized Grasping AutoEncoder (IGAE) takes an augmented image as input and performs reconstruction tasks. It reconstructs first the original (denoised) RGB image, then the box, and finally the gripper binary masks. In our settings, λ_1 is set to 1, λ_2 to 10, and λ_3 to 20.

solely on the reward signal by removing all intervention observation incentives introduced earlier. This increases the number of parameters to be learned, potentially resulting in slower training, reduced sample efficiency, and higher complexity in the RL algorithm.

D. Domain Randomization for Sim-to-Real Transfer

Training reinforcement learning agents in idealized simulation environments is not sufficient to transfer their policy into real world systems due to the sim-to-real gap [22], [23]. Simulations can not capture accurately the expected noise of the robot’s measurements neither the exact appearance, for instance, lightning conditions, of real robotic setups.

In the scope of our analysis, we focus on state representation abstractions that incentivize simulation-trained RL agents to solve the task both in simulation and on the real system. We adopt the core ideas from the RAD module [9] and Tobin et al. [24], which demonstrated successful agent transfer through domain randomization in both numerical and vision-based domains.

Domain randomization is applied in two distinct ways in the case of image inputs: 1) by directly adding noise to the images generated by the simulator, and 2) by first applying physical adaptations to the simulation environment and then introducing additional noise through step 1.

In the first step, the following augmentations are randomly applied: Random Cropping, Gaussian Blurring, Random Changes in Brightness, Random Four-Point Perspective Transform, and Random Channel-Wise Noise. Finally, for the second step, our simulator⁴ offers a wide range of physical adaptations to enhance realism and variability: Random Floor Appearance, Random Texture, Shadow Randomization, and Random Camera Pose Perturbations.

State Randomized RL Agent: In the case of numeric observations, a more conservative approach is followed since the manipulator’s encoders measurements are less noisy compared to the images. This agent is similar to the State RL Agent, with the difference that a uniform noise of 5% is

⁴The simulator used for the experiments is available at: <https://github.com/tum-i6/VTPRL>

applied at every time step t in the state of the agent during the policy training.

IV. EXPERIMENT SETUP

A. Environment Description

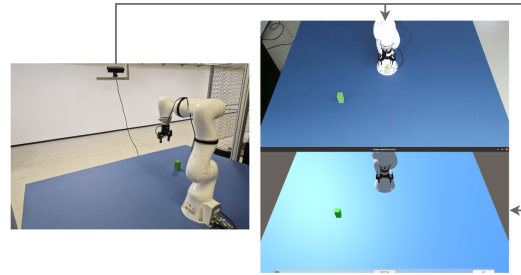


Fig. 4: Overview of the real world setup (left). Image observation from the Kinect V2 camera (top), and the aligned image observation in the simulated environment (bottom).

For the experiments we use the VTPRL simulation environment introduced in [25], developed with the Unity game engine [26] and coupled with the Dynamic Animation and Robotics Toolkit (DART) [27] for the inverse kinematics calculations. It has a comparable API to OpenAI Gym [28] and allows parallel simulation of several robots to speed-up the training process. We use the KUKA LBR iiwa 14 robotic manipulator [29] and the 2-Finger Adaptive Robotic Gripper (2F-85 model) by Robotiq [30], with maximal opening of 85 mm. The simulated manipulator and gripper parameters and meshes are obtained from the URDF data provided by the ROS-Industrial [31] and Robotiq [32] packages. The real robot is controlled with the IIWA stack [33] via Robot Operating System (ROS) [34]. In the real setup, the image observations are taken with the Microsoft Kinect V2 camera sensor [35] and processed with the `iai_kinect2` [36] package. The object we grasp is a foam box with dimensions of 50 x 100 x 50 mm (width x height x depth).

B. Implementation Details

AutoEncoders Implementation Details: The agents learning process here is divided into three separate steps:

1) training images and segmentation masks are initially generated from the simulation based on the unique color of the gripper and the target object, 2) the autoencoders are then trained to compress augmented (noisy) images into 128-dimensional latent vectors. This is achieved by reconstructing the original (denoised) RGB images, guided by an Mean Squared Error (MSE) loss objective. As a result, a simulated and a corresponding real-world image are encoded to similar latent representation. Additionally, to further shape the latent space, the IGAE predicts two binary masks with Binary Cross-Entropy (BCE) loss objectives: one for the gripper and one for the target object, and finally, 3) once the autoencoders have been optimized, the frozen encoders process the image observations and the agents learn a policy through interactions with the environment while relying on latent vector states.

RL Policy Details: For all representation spaces we used the model-free algorithm Proximal Policy Optimization (PPO) [37] to train the agents. This algorithm is particularly well-suited for continuous action spaces, and the novel proposed clipping coefficient can effectively address the high variance issues in the policy update step. We used the parallel PPO implementation from StableBaselines3 [38].

Regarding the architecture of the policy network, the default implementation for the PPO algorithm of the StableBaselines3 (2 fully connected layers of 64 units and Tanh activation functions for each of the the actor and the critic heads) showed the best performance. However, in the vision-based methods, replacing the Tanh with ReLUs activations yielded more stable results⁵.

The hyperparameters for the policies and encoders architectures were determined using the Optuna Search framework [39]. The policy optimization process was carried out on the State RL agent, and the best-found hyperparameters were also applied to the other agents. However, the learning rate (α), and clip range (ϵ), were optimized from the beginning in all approaches since these parameters are highly sensitive to the dimension of the representation, ensuring fair comparisons across the methods. The hyperparameter settings for PPO can be found in tables I and II.

TABLE I: Model-specific RL training hyperparameters.

	St.	St. (rnd.) & VtS	AE & IGAE	EtE
LR (α)	0.001	0.0005	0.0001	0.00005
Clip range (ϵ)	0.3	0.25	0.25	0.25

TABLE II: Shared RL training hyperparameters.

Entropy coefficient (c_2)	0.02
Discount factor (γ)	0.96
Bias-variance trade-off (λ)	0.92
Number of steps (n_steps)	512
Number of optimization epochs (n_epochs)	10
Value function coefficient (c_1)	0.5
Gradient Clipping (max_grad_norm)	0.5
Mini-batches ($batch_size$)	32

During training, the agents’ actions and states are scaled to fall within the range of $[-1, 1]$ for stability purposes. The maximum task-space velocities are also set to $0.035m/sec$, and the configured control cycle is $20Hz$. For the non-learning baseline, we intentionally remove the acceleration and jerk constraints to ensure a fair alignment with the RL definitions. To force the robotic manipulator to perform planar movements and maintain a consistent pose across its uncontrolled DoFs (4 in total), a Proportional (P)-controller is utilized. The gains are 0.5, and 1.5 for the positional and rotational errors, respectively. The same P-controller is employed across all different approaches.

⁵Most likely the sparsity property contributed to the improved behaviour, given the larger input dimension compared to the State RL agent. We also observed that other types of networks performed much worse, and smaller policy networks always outperformed larger ones in our setup.

The episode duration is uniform and set to 400 time steps, and the RL agents were trained for a total of 1.5 million time steps. The reward weights w_x and w_z are both set to a value of 1.0, and the collision term r_c to a value of -100 . The joint limits are set to -10° from the physical limits. We finally train on 16 environments in parallel, and for evaluation, 50 random box positions were selected to assess the 30 saved model checkpoints.

V. EXPERIMENT RESULTS

The success rate development during training of the RL agents, along with the non-learning baseline on the 50 evaluation boxes, is shown in Figure 5. These results consist of an average of 5 runs with distinct initialization seeds. The grasping task can be completely solved with a 100% success rate using the following methods: 1) Ruckig, 2) Ideal State and 3) Randomized State, and 4) IGAE RL agents.

The majority of approaches exhibit small standard deviations, with the exception of the vanilla autoencoder and end-to-end RL agents. In the Ideal State RL agent, after 180.000 time steps, the standard deviation across all five runs becomes zero. In the absence of errors and noise, numerical reinforcement learning agents can solve the task as good as non-learning control methods that have full system knowledge. However, by introducing only 5% of uniform random noise in the observation, i.e. the Randomized State RL agent, results in a 2x slower convergence rate.

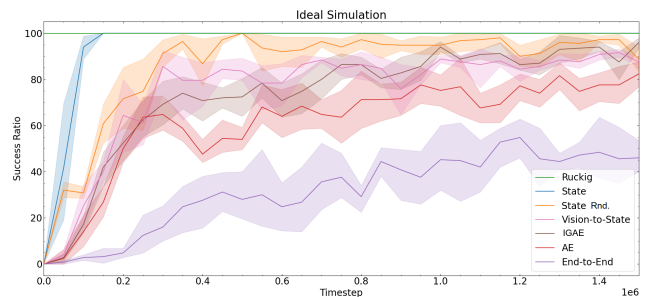


Fig. 5: The success rate development in simulation of the proposed agents, each utilizing distinct representation space.

The task-specific IGAE RL agent is the best performing vision-based method. We hypothesize that this is due to the additional object and end effector reconstruction heads, which induce a rich latent feature vector that can effectively incentivize the policy to understand the important parts of the environment. The VtS and vanilla AE agents then follow with success rates of 94% and 92%, respectively. However, when the best models are evaluated in a simulation environment with heavy random physical adaptations applied (e.g., camera position), the performance drops to 78% for the IGAE and 70% for both VtS and vanilla AE agents, as shown in the third column of Table III.

During the sim-to-real transfer, we evaluate the checkpoints for the vision-based models that perform best in randomized simulations to gain insights into the effectiveness of the proposed augmentations into bridging the sim-to-real gap.

On the real system, the Ruckig trajectory generation algorithm, along with both the Ideal and Randomized State RL trained models, consistently achieved successful picking of all 50 evaluation boxes. The top-performing vision-based agent in the real setup is the IGAE RL agent, with a success rate of 84%. In contrast, all other agents relying on image observations experienced a significant drop in their ability to grasp the targets. Specifically, the vanilla autoencoder achieved a success rate of 60%, followed by the VtS with 52%. The end-to-end paradigm exhibited the lowest success rate, at 24%.

In qualitative terms, as it is evident in the supplementary video, the Randomized State RL agent exhibited smoother behavior compared to the Ideal State agent. It maintained minimal velocities when approaching the boxes, while the Ideal State agent displayed a jittery movement pattern due to operating at maximum velocity ranges, resulting in overshooting. This highlights the importance of incorporating observation noise during policy training for numerical agents to ensure robust sim-to-real transfer.

TABLE III: Mean success rate across the different state representation strategies.

Strategy	Average in Idl. Simulation	Best Model (Idl. Sim.)	Best Model (Rnd. Sim.)	Best Model (Real)
Ruckig	100%	100%	N/A	100%
St.	100%	100%	N/A	100%
St. (rnd.)	100%	100%	N/A	100%
VtS	91.6% \pm 2.2	94%	70%	52%
IGAE	96.0% \pm 2.8	100%	78%	84%
AE	82.4% \pm 7.1	92%	70%	60%
EtE	54.8% \pm 11.0	78%	44%	24%

VI. DISCUSSION

The results show significant difference in performance between RL agents relying on numerical vs. image-based representations. Since solving the task requires high precision, a representation generated from the robot’s encoders is more suitable to learn from, compared to a more abstract representation inferred from images. The performance of image-based representations can be improved if we introduce domain knowledge and provide an incentive about the important aspects of the task, as it is done with the IGAE approach. Otherwise, a vanilla autoencoder would assign equal importance to all pixels in the input observations. This is a problem in the specific case, because the robot and the box occupy a small portion of the workspace, making the latent vectors more prone to noise. However, general representations like the ones generated from the vanilla autoencoder become crucial in scenarios where searching for suitable objectives (intervention incentives) to shape the original representation space is not straightforward. For instance, in tasks like pushing objects in cluttered scenes or collaborative tasks, where defining precise objectives can be challenging.

The results provide empirical evidence that decoupling the representation learning from the policy learning leads to better performance. In the case of end-to-end learning, both the encoder and policy network weights are back-propagated

during the policy update steps, and the only signal to refine the state of the agent is the reward function. In future works, intervention incentives for control, like action primitives [40], should be considered to reduce again the optimization difficulty of the RL policy.

It seems also that even small errors in the prediction of the state from the VtS agent could lead to detrimental results. A minor error of 2° could result in an average error of 5 cm in task-space for a 1.5 m robot and lose the target. Noisy predictions is some of the dimensions of the 128-dim latent vectors of the autoencoders do not affect at the same level the agent behaviour. It would be more practical instead to regress the pose of the end effector, where the predictions could be more precise.

Finally it is plausible that by fine-tuning the individual networks, such as carefully designing the architectures of the neural networks in VtS and end-to-end approaches and optimizing all the policy hyperparameters of the PPO algorithm from the beginning, could lead to higher success rates for the grasping task. However, we focused on ensuring equal conditions as much as possible throughout the approaches to examine the advantages and weaknesses of each approach more objectively.

VII. CONCLUSION AND FUTURE WORK

In this study, we provided practical insights on the complex relationship between state representation in reinforcement learning, available system and environment information, and sim-to-real transfer. Using a grasping task that is easy to solve for a model-based approach with full system knowledge, we examined how well an RL agent that uses a representation with an increasing level of abstraction can solve the same task. While RL agents with hand-crafted representation had 100% success, it was challenging to solve the task from images considering the high precision needed in combination with the low resolution image input and the simulation-only training. We found that autoencoder-based methods need to be incentivised with domain knowledge to provide a robust representation for solving the task. An RL agent relying on representation from our proposed Incentivized Grasping AutoEncoder could completely solve the task in simulation, and achieved a success rate of 84% in sim-to-real transfer.

In future work, we would like to further explore the potential of autoencoders and other general representation learning approaches in complex tasks, where RL agents should possess the flexibility to discern the critical aspects of the environment they operate in and relying on user-defined and hard-coded state representations can constrain the agents adaptability. Through tasks that require rich contact, like grasping in cluttered scenes, object pushing or interaction with novel objects, as well as through architectures like vision transformers, we anticipate gaining deeper insights into the most effective state representation approaches for robotics applications.

REFERENCES

- [1] Y. Tassa, Y. Doron, A. Muldal, T. Erez, Y. Li, D. de Las Casas, D. Budden, A. Abolmaleki, J. Merel, A. Lefrancq, T. P. Lillicrap, and M. A. Riedmiller, "Deepmind control suite," *CoRR*, vol. abs/1801.00690, 2018. [Online]. Available: <http://arxiv.org/abs/1801.00690>
- [2] T. Everitt, R. Carey, E. D. Langlois, P. A. Ortega, and S. Legg, "Agent incentives: A causal perspective," *Proceedings of the AAAI Conference on Artificial Intelligence*, vol. 35, no. 13, pp. 11487–11495, May 2021. [Online]. Available: <https://ojs.aaai.org/index.php/AAAI/article/view/17368>
- [3] T. Everitt, P. A. Ortega, E. Barnes, and S. Legg, "Understanding agent incentives using causal influence diagrams. part i: Single action settings," 2022.
- [4] A. Tirinzoni, M. Papini, A. Touati, A. Lazaric, and M. Pirota, "Scalable representation learning in linear contextual bandits with constant regret guarantees," in *Advances in Neural Information Processing Systems*, S. Koyejo, S. Mohamed, A. Agarwal, D. Belgrave, K. Cho, and A. Oh, Eds., vol. 35. Curran Associates, Inc., 2022, pp. 2307–2319. [Online]. Available: https://proceedings.neurips.cc/paper_files/paper/2022/file/0fd489e5e393f61b355be86ed4c24a54-Paper-Conference.pdf
- [5] C. Dann, Y. Mansour, M. Mohri, A. Sekhari, and K. Sridharan, "Guarantees for epsilon-greedy reinforcement learning with function approximation," in *International Conference on Machine Learning, ICML 2022, 17-23 July 2022, Baltimore, Maryland, USA*, ser. Proceedings of Machine Learning Research, K. Chaudhuri, S. Jegelka, L. Song, C. Szepesvári, G. Niu, and S. Sabato, Eds., vol. 162. PMLR, 2022, pp. 4666–4689. [Online]. Available: <https://proceedings.mlr.press/v162/dann22a.html>
- [6] A. Agarwal, S. Kakade, A. Krishnamurthy, and W. Sun, "Flambe: Structural complexity and representation learning of low rank mdps," in *Advances in Neural Information Processing Systems*, H. Larochelle, M. Ranzato, R. Hadsell, M. Balcan, and H. Lin, Eds., vol. 33. Curran Associates, Inc., 2020, pp. 20095–20107. [Online]. Available: https://proceedings.neurips.cc/paper_files/paper/2020/file/e894d787e2fd6c133af47140aa156f00-Paper.pdf
- [7] M. Uehara, X. Zhang, and W. Sun, "Representation learning for online and offline RL in low-rank MDPs," in *International Conference on Learning Representations*, 2022. [Online]. Available: <https://openreview.net/forum?id=J4iSIR9fhY0>
- [8] X. Zhang, Y. Song, M. Uehara, M. Wang, W. Sun, and A. Agarwal, "Efficient reinforcement learning in block mdps: A model-free representation learning approach," in *International Conference on Machine Learning*, 2022.
- [9] M. Laskin, K. Lee, A. Stooke, L. Pinto, P. Abbeel, and A. Srinivas, "Reinforcement learning with augmented data," in *Proceedings of the 34th International Conference on Neural Information Processing Systems*, ser. NIPS'20. Red Hook, NY, USA: Curran Associates Inc., 2020.
- [10] T. Haarnoja, A. Zhou, P. Abbeel, and S. Levine, "Soft actor-critic: Off-policy maximum entropy deep reinforcement learning with a stochastic actor," in *Proceedings of the 35th International Conference on Machine Learning*, ser. Proceedings of Machine Learning Research, J. Dy and A. Krause, Eds., vol. 80. PMLR, 10–15 Jul 2018, pp. 1861–1870. [Online]. Available: <https://proceedings.mlr.press/v80/haarnoja18b.html>
- [11] J. Josifovski, M. Malmir, N. Klarmann, B. L. Žagar, N. Navarro-Guerrero, and A. Knoll, "Analysis of randomization effects on sim2real transfer in reinforcement learning for robotic manipulation tasks," in *2022 IEEE/RSJ International Conference on Intelligent Robots and Systems (IROS)*, 2022, pp. 10193–10200.
- [12] S. Parisi, A. Rajeswaran, S. Purushwalkam, and A. K. Gupta, "The unsurprising effectiveness of pre-trained vision models for control," in *International Conference on Machine Learning*, 2022.
- [13] J. Deng, W. Dong, R. Socher, L.-J. Li, K. Li, and L. Fei-Fei, "Imagenet: A large-scale hierarchical image database," in *2009 IEEE conference on computer vision and pattern recognition*. Ieee, 2009, pp. 248–255.
- [14] S. Joshi, S. Kumra, and F. Sahin, "Robotic grasping using deep reinforcement learning," in *2020 IEEE 16th International Conference on Automation Science and Engineering (CASE)*, 2020, pp. 1461–1466.
- [15] M. Breyer, F. Furrer, T. Novkovic, R. Y. Siegwart, and J. I. Nieto, "Flexible robotic grasping with sim-to-real transfer based reinforcement learning," *ArXiv*, vol. abs/1803.04996, 2018.
- [16] A. Nair, S. Bahl, A. Khazatsky, V. Pong, G. Berseth, and S. Levine, "Contextual imagined goals for self-supervised robotic learning," in *Conference on Robot Learning (CoRL)*, 2019.
- [17] A. Zhan, R. Zhao, L. Pinto, P. Abbeel, and M. Laskin, "Learning visual robotic control efficiently with contrastive pre-training and data augmentation," 2022.
- [18] C. S. Wickramasinghe, D. L. Marino, and M. Manic, "Resnet autoencoders for unsupervised feature learning from high-dimensional data: Deep models resistant to performance degradation," *IEEE Access*, vol. 9, pp. 40511–40520, 2021.
- [19] S. Levine, C. Finn, T. Darrell, and P. Abbeel, "End-to-end training of deep visuomotor policies," *The Journal of Machine Learning Research*, vol. 17, no. 1, pp. 1334–1373, 2016.
- [20] P. Florence, L. Manuelli, and R. Tedrake, "Self-supervised correspondence in visuomotor policy learning," *IEEE Robotics and Automation Letters*, vol. PP, pp. 1–1, 11 2019.
- [21] L. Berscheid and T. Kröger, "Jerk-limited real-time trajectory generation with arbitrary target states," *Robotics: Science and Systems XVII*, 2021.
- [22] W. Zhao, J. P. Queralta, and T. Westerlund, "Sim-to-real transfer in deep reinforcement learning for robotics: a survey," in *2020 IEEE Symposium Series on Computational Intelligence (SSCI)*, 2020, pp. 737–744.
- [23] M. Malmir, J. Josifovski, N. Klarmann, and A. Knoll, "Robust sim2real transfer by learning inverse dynamics of simulated systems," in *2nd Workshop on Closing the Reality Gap in Sim2Real Transfer for Robotics*, 2020.
- [24] J. Tobin, R. Fong, A. Ray, J. Schneider, W. Zaremba, and P. Abbeel, "Domain randomization for transferring deep neural networks from simulation to the real world," in *2017 IEEE/RSJ International Conference on Intelligent Robots and Systems (IROS)*, 2017, pp. 23–30.
- [25] J. Josifovski, M. Malmir, N. Klarmann, and A. Knoll, "Continual Learning on Incremental Simulations for Real-World Robotic Manipulation Tasks," in *2nd R:SS Workshop on Closing the Reality Gap in Sim2Real Transfer for Robotics*, Corvallis, OR, USA, 2020, p. 3.
- [26] "Unity 3d," <https://unity.com/>, accessed: 2020-6-26.
- [27] J. Lee, M. X. Grey, S. Ha, T. Kunz, S. Jain, Y. Ye, S. S. Srinivasa, M. Stilman, and C. K. Liu, "Dart: Dynamic animation and robotics toolkit," *Journal of Open Source Software*, vol. 3, no. 22, p. 500, 2018. [Online]. Available: <https://doi.org/10.21105/joss.00500>
- [28] G. Brockman, V. Cheung, L. Pettersson, J. Schneider, J. Schulman, J. Tang, and W. Zaremba, "OpenAI Gym," *arXiv:1606.01540 [cs]*, 2016.
- [29] "Kuka lbr-iiwa," <https://www.kuka.com/products/robot-systems/industrial-robots/lbr-iiwa>, accessed: 2020-6-26.
- [30] "robotiq: 32f-85 robot gripper," <https://robotiq.com/products/2f85-140-adaptive-robot-gripper>.
- [31] "Ros industrial," https://github.com/ros-industrial/kuka_experimental, accessed: 2022-2-23.
- [32] "Robotiq packages," <https://github.com/ros-industrial/robotiq>, accessed: 2013-10-13.
- [33] C. Hennemperger, B. Fuerst, S. Virga, O. Zettinig, B. Frisch, T. Neff, and N. Navab, "Towards MRI-Based Autonomous Robotic Us Acquisitions: A First Feasibility Study," *IEEE Transactions on Medical Imaging*, vol. 36, no. 2, pp. 538–548, 2017.
- [34] Stanford Artificial Intelligence Laboratory et al., "Robotic operating system." [Online]. Available: <https://www.ros.org>
- [35] P. Fankhauser, M. Bloesch, D. Rodriguez, R. Kaestner, M. Hutter, and R. Siegwart, "Kinect v2 for mobile robot navigation: Evaluation and modeling," in *2015 international conference on advanced robotics (ICAR)*. IEEE, 2015, pp. 388–394.
- [36] T. Wiedemeyer, "IAI Kinect2," https://github.com/code-iai/iai_kinect2, Institute for Artificial Intelligence, University Bremen, 2014 – 2015, accessed June 12, 2015.
- [37] J. Schulman, F. Wolski, P. Dhariwal, A. Radford, and O. Klimov, "Proximal policy optimization algorithms," 2017.
- [38] A. Raffin, A. Hill, A. Gleave, A. Kanervisto, M. Ernestus, and N. Dormann, "Stable-baselines3: Reliable reinforcement learning implementations," *Journal of Machine Learning Research*, vol. 22, no. 268, pp. 1–8, 2021. [Online]. Available: <http://jmlr.org/papers/v22/20-1364.html>
- [39] T. Akiba, S. Sano, T. Yanase, T. Ohta, and M. Koyama, "Optuna: A next-generation hyperparameter optimization framework," in *Proceedings of the 25th ACM SIGKDD International Conference on Knowledge Discovery and Data Mining*, 2019.
- [40] M. Dalal, D. Pathak, and R. Salakhutdinov, "Accelerating robotic reinforcement learning via parameterized action primitives," in *NeurIPS*, 2021.

APPENDIX

A. NUMERICAL AGENTS AND STATE RANDOMIZATION

Figure 6 illustrates the trajectories followed by the end effector in x and y-axes, correspondingly, for numerical reinforcement learning agents. An agent trained in simulation without state randomization applied, can not stabilize at the target position defined by the fourth evaluation box with coordinates $(-0.26, 0.54)$. It presented oscillatory motion with overshooting. The Randomized Numerical RL agent achieved a total return of 40.69, outperforming the Ideal Numerical RL agent with 39.85 total return. The difference is significant since the average return is approximately 0.02 per time step.

As demonstrated also in the study of Laskin et al. [9], carefully designed state randomization during policy training is necessary for enabling successful RL agents transfer to real-world systems.

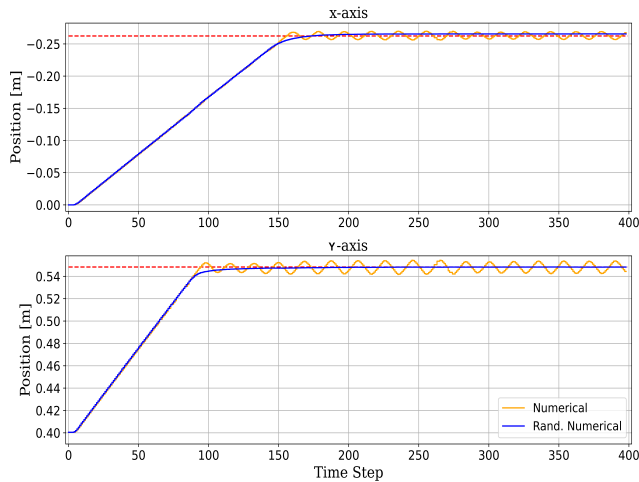


Fig. 6: The plot depicts the trajectories followed by numerical reinforcement learning agents, comparing them under two conditions: one with state randomization noise and one without. The goal is to reach the fourth evaluation box.